Chapter 20

Resonators for Annular Gain Media

20.1 Characteristics of Annular Gain Lasers

In high power gas and solid state lasers the maximum output power is limited by the efficiency of heat removal. The temperature rise associated with the heat generated by the pump process leads to a decrease of the stimulated emission cross section and an increase of the lower laser level population. For sealed-off CO_2 lasers in cylindrical geometry, these effects reduce the maximum output power per length to about 80W/m, independent of the tube diameter. Furthermore, in solid state laser materials, the pump induced stress causes irreversible damage to the medium if the pump power is increased beyond the fracture limit. The experimentally established fracture limit of flashlamp pumped and diode-pumped Nd:YAG rod allows up to 40W and 60Wof output power per cm of rod length, respectively.

Lower temperatures and higher fracture limits can be attained by choosing a geometry of the gain medium that exhibits a larger surface to volume ratio than the cylindrical geometry. Besides the slab geometry (see Sec. 19.2), an annular active medium provides a much larger cooling surface than a rod of equal volume. If a and b denote the inner and outer radii of the annulus, respectively, the maximum output power P_A that can be extracted from an annular gain medium reads [5.162,5.167]:

$$P_A = P_R \, 2 \, \frac{b+a}{b-a} \qquad \textit{for gas lasers} \tag{20.1}$$

$$P_A = P_R \, \frac{3}{2} \, \frac{b+a}{b-a} \qquad \textit{for solid state lasers} \tag{20.2}$$

where P_R is the maximum output power attainable for a rod (or gas tube) of equal length, and b-a is much smaller than a. The power scaling is different for gas and solid state lasers due to the physical mechanisms involved. In gas lasers, the output power is limited by the gas temperature, whereas in solid state materials the surface stress has to remain below the fracture limit. For an inner radius of 30mm and a wall thickness of 5mm, an annular gas medium provides a 26 times higher output power per length compared to a conventional tube. Annular gain media have been realized in dye lasers and He-Xe lasers [5.131,5.137], HF lasers [5.134], CO_2 lasers [5.133,5.135,5.141,5.151,5.163-5.170], Nd:glass lasers [5.130], and Nd:YAG lasers [5.157,5.158,5.161,5.162] (Figs.20.1, 20.2). A maximum output power of 1.86kW was reported for an inside pumped Nd:YAG tube laser (tube

length: 130mm, R_i=*17.5mm*, R_o=*26.5mm*)[5.162]. An output power of 1kW was achieved with a sealed-off CO_2 laser (electrode length: 1.15m, R_i=*48mm*, R_o=*55mm*) [5.170]. Both systems operated at a total efficiency of 10%.

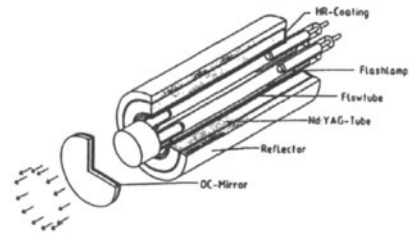

a)

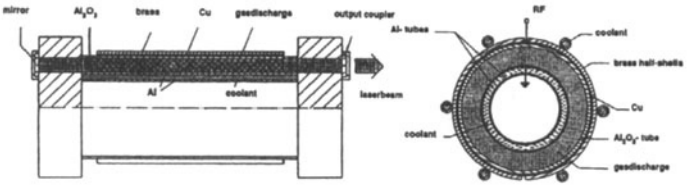

b)

Fig. 20.1 a) Nd:YAG laser [5.157] (© OSA 1991) and b) CO_2 laser with annular gain medium [S.23].

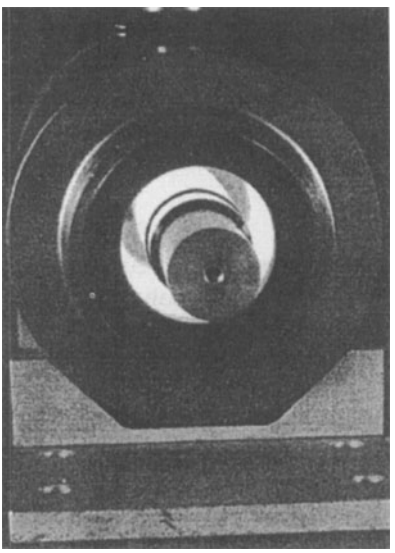

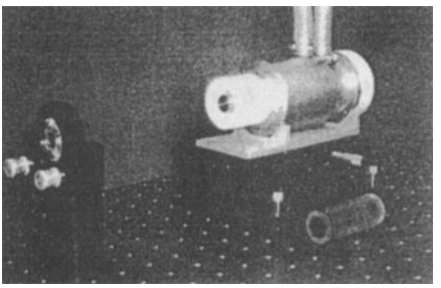

Fig. 20.2 Inside pumped Nd:YAG tube laser providing an average output power of 1.8kW at a total efficiency of 10%. The left photograph is a front view of the tube with the four flashlamps in simmer operation. The upper photograph presents a side view of the laser head including the output coupling mirror . The rear endface of the tube is HR coated [5.157,5.158] (courtesy of Laser- und Medizin-Technologie Berlin gGmbH, Germany).

Although the tube geometry is very well suited to provide high output powers, this concept has not yet found commercial application. This is not only due to the more sophisticated, and therefore more expensive, laser head design. The main problem of the annular geometry is the realization of good beam quality without decreasing the output power too much. A variety of optical resonators suitable for annular gain media have been studied in the last two decades. Nevertheless, none of these resonator schemes are capable of providing beam properties that would justify a replacement of commercial rod or slab lasers. In the following, an overview of the performance of different annular resonator schemes is given.

20.2 Stable Resonators with Toric Mirrors

20.2.1 Transverse Mode Structure

Resonators with toric mirrors exhibit mode structures similar to those of conventional spherical mirror resonators. Both mirrors exhibit a radius of curvature ρ_i in the radial direction and are flat in the azimuthal direction (Fig. 20.3). Both stable and unstable resonators can be realized [5.133,5.146]. The resonator properties are determined by the g-parameters $g_i=1-L/\rho_i$, the effective resonator length L, the inner radius a, and the wall thickness of the tube $d=b-a$. If the toric mirror resonator is unwound, a one dimensional strip resonator is obtained (Fig.20.4). The circumference of the annular mirrors is now represented by the height of the cylindrical mirrors. For a large radius r_0 of the mirror vertex, the radial modes of the unconfined stable toric resonator can therefore be approximated by one-dimensional Gauss-Hermite modes [5.153]. In this so-called slab approximation, the mode diameter and the number of oscillating radial modes can be calculated by using the well-known relationships for conventional resonators in rectangular symmetry. However, in general, the vertex diameter is not large enough to neglect the influence of the bending on the radial mode structure. In this case, the transformation from a cylindrical to a toric mirror shifts the radial intensity maxima slightly inward.

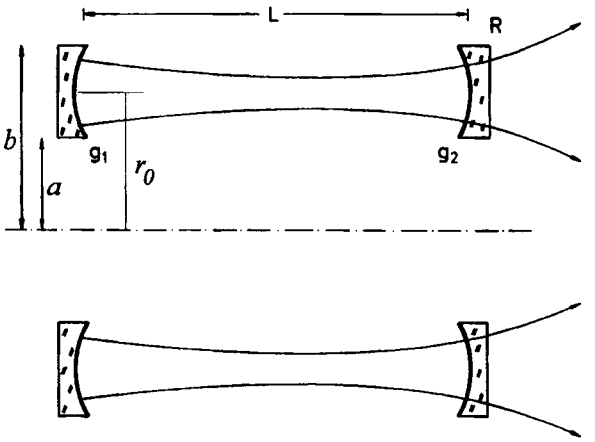

Fig. 20.3 Stable resonator with toric mirrors (cross sectional view).

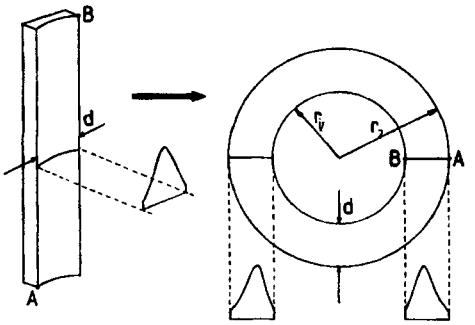

Fig. 20.4 A toric mirror is generated by bending a cylindrical mirror. For vertex diameters r_1+r_2 that are much larger than the mirror width d, the radial mode structures of toric resonators are similar to those of resonators in rectangular geometry.

If both mirrors are unconfined, the field distributions of the transverse eigenmodes of passive toric mirror resonators can be calculated analytically [5.153,5.160]. In polar coordinates, the field distributions read:

$$E_{pl}(r,\phi) \propto \frac{1}{\sqrt{r}} \exp\left[-\frac{(r-r_0)^2}{w_0^2}\right] H_p\left[\frac{\sqrt{2}(r-r_0)}{w_0}\right] \exp[\pm il\phi] \qquad (20.3)$$

where p,ℓ are the radial and the azimuthal mode index ($p,\ell \geq 0$), respectively, r_0 is the radius of the mirror vertex, w_0 is the Gaussian beam radius, and $H_p[x]$ is the Hermite polynomial of order p. Note that for large vertex radii r_0 and small beam diameter, the influence of the factor $1/\sqrt{r}$ on the mode structure becomes negligible. This is the mathematical representation of the slab approximation. The radial intensity distributions can then be approximated by Gauss-Hermite polynomials.

If both mirrors are unconfined, the beam radius of the transverse modes depends only on the radial mode order p. Thus, the transverse modes are highly degenerate and the simultaneous oscillation of on the order of a hundred azimuthal modes is to be expected. This also holds true if the mirrors are limited by annular apertures. The numerical investigation of the diffraction integral for a resonator round trip reveals that the azimuthal mode discrimination remains weak, although the radial mode structure now depends on the azimuthal index [5.163]. The radial mode profile is shifted outward as the azimuthal mode index is increased, resulting in an increase in the diffraction losses. Figure 20.5 presents numerically calculated round trip losses of the modes with $p=0$ as a function of the azimuthal order for symmetric toric stable resonators. The azimuthal mode discrimination increases with the mirror curvature and the mode with $\ell=0$ experiences the lowest loss if the mirror vertex is in the center of the annular gap. However, the losses are nearly degenerate for low order modes.

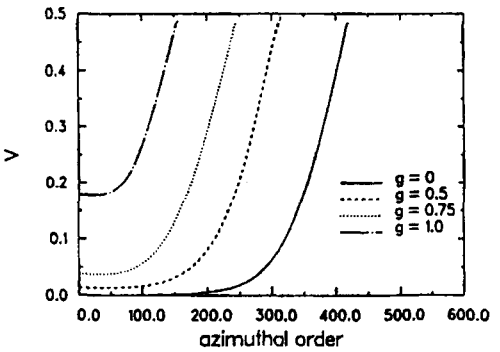

Fig. 20.5 Calculated diffraction losses per round trip for the fundamental radial mode (p=0) of symmetric toric resonators as a function of the azimuthal mode order. The curve parameter is the g-parameter of the mirrors. The mirror vertex is centered with the annular gap. Vertex radius r_0=50mm, resonator length L=1m, wavelength λ=10.6μm, gap width b-a=6mm [5.163] (© OSA 1993).

The loss minimum can be shifted towards higher azimuthal orders if the radius r_0 of the mirror vertex is chosen smaller than the radius $(a+b)/2$ of the gap center. This will improve the azimuthal mode discrimination, but, unfortunately, will also prevent circularly symmetric modes ($\ell=0$) from oscillating. This is a major drawback because only the modes with $\ell=0$ exhibit a centered intensity profile in the far field. The azimuthal index ℓ of the lowest loss mode for symmetric resonators is given by [5.163]:

$$\ell = \frac{\pi(a+b)^2}{2\lambda L}\sqrt{2(1-g)\left(1-\frac{2r_0}{a+b}\right)} \tag{20.4}$$

where g is the g-parameter of the resonator mirrors and λ is the wavelength.

19.2.2 Beam Quality

The beam quality of toric stable resonators is determined by the mode with the highest radial mode order p and only slightly depends on the azimuthal structure. Similar to conventional resonators, the highest mode order can be found by adapting the beam diameter to the gap width of the annular aperture:

$$w_{00}\sqrt{p+1} \approx \frac{b-a}{2} \tag{20.5}$$

where w_{00} is the Gaussian beam radius at the aperture.

The beam waist w_p of this radial mode and the corresponding half angle of divergence θ_p can then be directly calculated using the expressions derived in Chapter 5. However, the waist radius w of the laser beam is given by the outer radius of the annular intensity distribution and not by the radius w_p of the mode profile in the annular gap. For a given mode order, the beam parameter product, therefore, is higher than for conventional resonators. In a geometrical approximation, the laser beam waist radius is larger than the waist radius of the radial mode in the annular gap by the factor *2b/(b-a)*, where *a,b* are the inner and the outer radii of the annular aperture, respectively. Thus, the beam parameter product can be approximated by:

$$w\theta = \frac{2b}{b-a} w_p \theta_p = (p+1) \frac{2b}{b-a} \frac{\lambda}{\pi} \tag{20.6}$$

where θ is the half angle of divergence. Figure 20.6 presents calculated radial intensity distributions in the near field and the far field of the fundamental mode for a toric resonator with different inner diameters of the annulus. The annular shape of the near field generates a high power content in the side lobes of the far field. An on- axis intensity maximum in the far field is only found for modes without azimuthal structure (ℓ=0). For higher azimuthal orders, the far field intensity distribution remains annular since all waves originating from the annular medium interfere destructively on the optical axis. Considering the lack of azimuthal mode discrimination, it is no surprise that measured far field intensity distributions of toric resonators generally contain most of the power in an annular ring (Fig. 20.6).

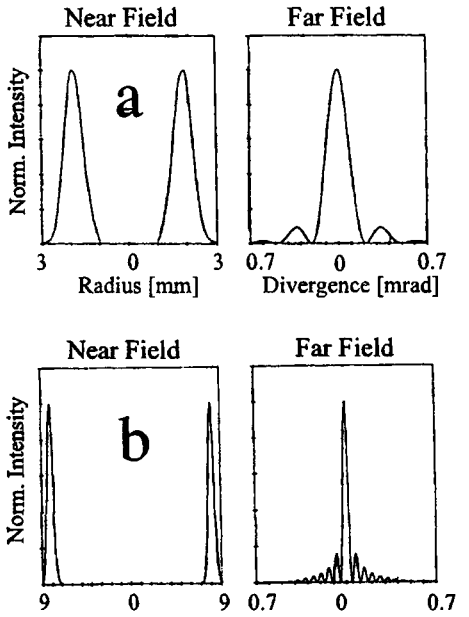

Fig. 20.6 Calculated intensity distributions of the TEM_{00} mode for a semi-confocal toric resonator (g_1=1, g_2=*0.5*, *L=0.5m*, λ=*1.06μm*). The normalized intensity distributions at the flat mirror and in the far field are shown for two different tube dimensions. a) *a=1mm*, *b=3mm*, b) *a=7mm*, *b=9mm*.

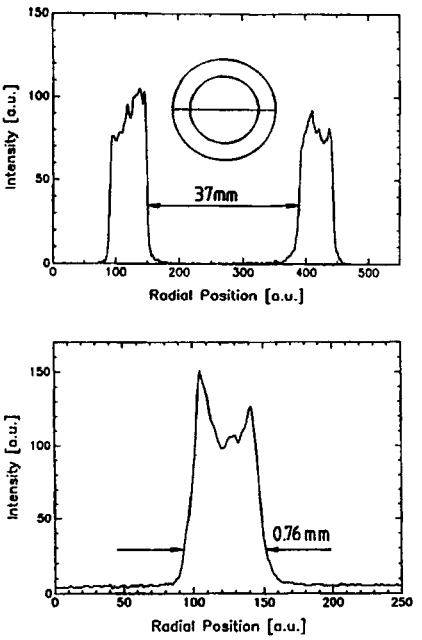

Fig. 20.7 Recorded radial intensity profiles in the near field and the far field of a Nd:YAG tube laser with a flat-flat resonator (tube dimensions: a=17.5mm, b=26.5mm, tube length: 100mm, resonator length: 1.2m). The equivalent resonator is toric due to the thermal lensing of the tube. The far field was recorded in the focal plane of a 200mm lens. The beam parameter product is 50 mm mrad (pump power: 3kW, output power: 200W) [5.158] (© AT Fachverlag 1991).

The beam quality of annular laser beams can be improved by reducing the diameter of the central hole without increasing the beam divergence. This is not in contradiction with Liouville's Theorem because the area in phase space is not decreased. The removal of the central hole can be accomplished by an axicon telescope, as shown in Fig. 20.8. The beam parameter product is reduced by the same factor as the outer beam diameter. However, the axicon telescope only preserves the beam divergence if the azimuthal mode index is low. Calculated beam parameter products with and without the axicon telescope are presented in Fig. 20.8. This figure indicates that the beam quality will only be significantly improved if the azimuthal mode order is lower than about twice the radial mode index. Note that without the axicon telescope, the beam parameter product is almost independent of the azimuthal mode order.

In summary, toric resonators are not very suitable for annular gain lasers due to the low azimuthal mode discrimination. Even if fundamental mode operation in the radial direction can be attained (like in CO_2 lasers), the oscillation of higher order azimuthal modes results in an annular far field. Furthermore, due to the annular shape of the near field, the beam parameter product is an order of magnitude higher than for a conventional Gaussian beam. The goal of annular resonator design, therefore, is to break the circular symmetry of the near field by generating a compact output beam at one side of the annular medium. This not only eliminates the deterioration of the beam quality due to the annular geometry, but also prevents the formation of ring patterns in the far field. One such resonator scheme is the Multipass Herriot Cell.

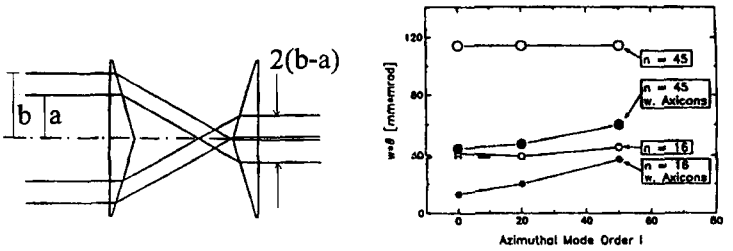

Fig. 20.8 Calculated reduction of the beam parameter product for an annular beam of a stable toric resonator with inner radius $a=17.5mm$ and outer radius $b=26.5mm$ as a function of the azimuthal mode order ℓ. The results for two different radial mode orders n, both with and without the axicon telescope, are shown. The beam parameter product is defined via the 86.5% power content (numerical calculation using diffraction integrals) [S.24].

20.3 Herriot Cell Resonators

A common resonator used in annular CO_2 lasers to extract the power in a compact, low order transverse mode is the Herriot cell resonator [5.127,5.149,5.151,5.156]. The Herriot cell can be viewed as a folded, linear resonator that generates multiple passes through the medium (Fig.20.9). The two high reflecting spherical mirrors with off-axis apertures form an optical delay line. The number of reflections and the orientation of the beams can be controlled by the mirror curvatures, the mirror distances, the location of the apertures, and the inclination of the incident beam [5.126,5.140,5.154]. In general, the reflected beams trace an elliptical curve on each mirror, but for special geometries the beams lie on a surface of a hyperboloid of revolution and the intersecting points move around the mirror in a circular pattern. The number of reflections can be increased by increasing the radius of curvature of the mirrors. There are several constraints in the design of Herriot cell resonators. The beam diameter has to be adapted to the wall thickness of the tube and with each round trip in the Herriot cell, and the beam has to be shifted in the azimuthal direction by slightly more than its diameter. Furthermore, laser oscillation between the two high reflecting folding mirrors has to be prevented by inserting a multi-segment aperture that generates losses for fields that do not propagate along the intended beam path. The output power of optimized Herriot cell resonators typically is 40% lower as compared to resonators with toric or spherical mirrors. This is due to diffraction losses generated at the apertures and the incomplete filling of the gain medium. An experimental example is shown in Fig. 20.10 for a linearly folded Herriot cell resonator. Furthermore, wavefront aberrations induced by the active medium sum up due to the high number of transits, resulting in increased diffraction losses. The Herriot cell resonator, therefore, is not suitable for annular solid state lasers.

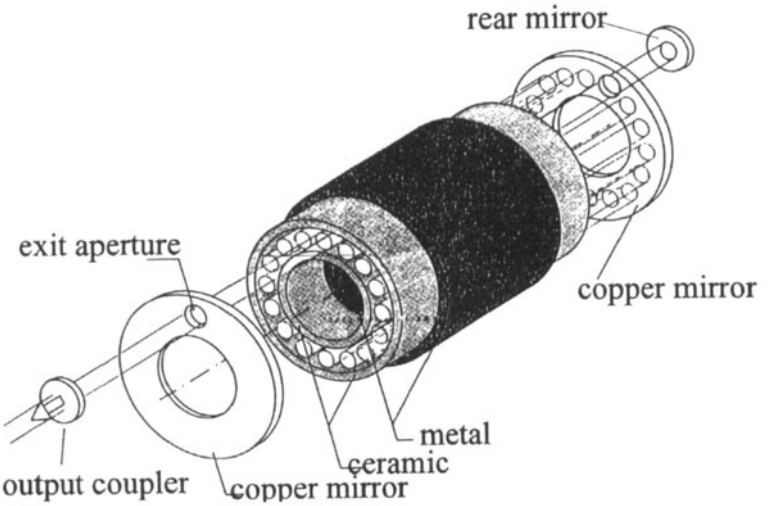

Fig. 20.9 Herriot cell resonator for an annular CO_2 laser [S.25].

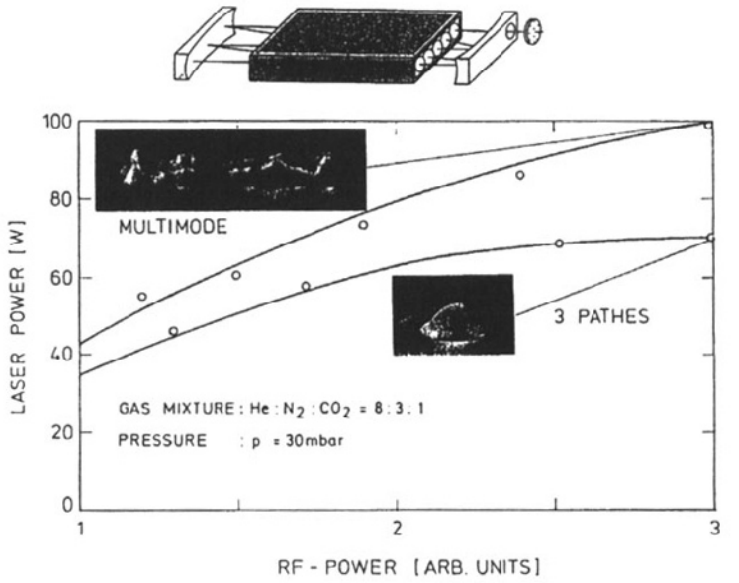

Fig. 20.10 Measured output power for a linear Herriot cell resonator with three passes in comparison to the output power attained with a conventional resonator. The upper graph presents the resonator scheme (with 5 passes) [S.25].

The beam propagation in Herriot cells can be mathematically described with ray transfer matrices [5.126,5.127,5.140,5.154]. Let us assume that a ray is launched into the Herriot cell at the point (x_0,y_0) with inclination angles (α_0,β_0) (Fig. 20.11). For a symmetric Herriot cell comprised of two spherical mirrors with radius of curvature ρ, the ray transfer matrix for a round trip reads:

$$\boldsymbol{M} = \begin{pmatrix} 1 & 0 \\ -2/\rho & 1 \end{pmatrix}\begin{pmatrix} 1 & L \\ 0 & 1 \end{pmatrix}\begin{pmatrix} 1 & 0 \\ -2/\rho & 1 \end{pmatrix}\begin{pmatrix} 1 & L \\ 0 & 1 \end{pmatrix}$$

$$= \begin{pmatrix} 2g-1 & 2Lg \\ 4g(g-1)/L & 4g^2-2g-1 \end{pmatrix} \tag{20.7}$$

where $g=1-L/\rho$ is the g-parameter of the mirrors and L is the mirror distance. After m round trips the ray vectors are given by:

$$\begin{pmatrix} x_m \\ \alpha_m \end{pmatrix} = \boldsymbol{M}^m \begin{pmatrix} x_0 \\ \alpha_0 \end{pmatrix} \quad , \quad \begin{pmatrix} y_m \\ \beta_m \end{pmatrix} = \boldsymbol{M}^m \begin{pmatrix} y_0 \\ \beta_0 \end{pmatrix} \tag{20.8}$$

(20.9)

Application of Sylvester's Theorem (1.46) yields for the ray transfer matrix:

$$\boldsymbol{M}^m = \frac{1}{\sin\Phi}\begin{pmatrix} (2g-1)\sin[m\Phi]-\sin[(m-1)\Phi] & 2Lg\sin[m\Phi] \\ 4g(g-1)\sin[m\Phi]/L & (4g^2-2g-1)\sin[m\Phi]-\sin[(m-1)\Phi] \end{pmatrix}$$

$$= \begin{pmatrix} A_m & B_m \\ C_m & D_m \end{pmatrix} \quad , \quad \sin\Phi = 2g\sqrt{1-g^2} \tag{20.10}$$

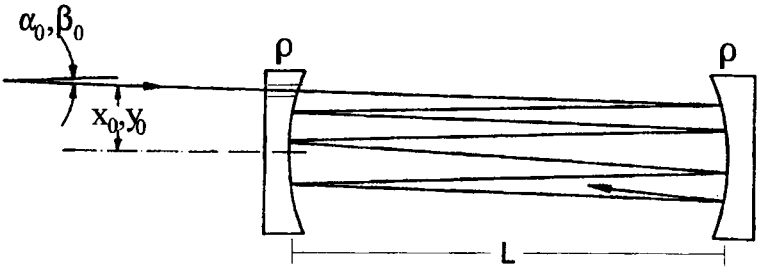

Fig. 20.11 Ray propagation in a symmetric Herriot cell.

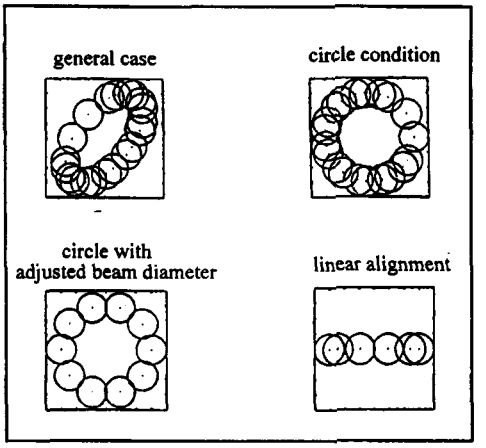

Fig. 20.12 Spot pattern on one mirror of the Herriot cell [S.26].

The coordinates of the ray after m round trips are given by:

$$x_m = A_m x_0 + B_m \alpha_0 \tag{20.11}$$

$$y_m = A_m y_0 + B_m \beta_0 \tag{20.12}$$

These two equations can be rewritten as:

$$x_m = R_x \sin(m\Phi + \delta_x) \tag{20.13}$$

$$y_m = R_y \sin(m\Phi + \delta_y) \tag{20.14}$$

with:

$$R_x^2 = x_0^2 + \frac{(\alpha_0 L + x_0(1-g))^2}{1-g^2} \tag{20.15}$$

$$R_y^2 = y_0^2 + \frac{(\beta_0 L + y_0(1-g))^2}{1-g^2} \tag{20.16}$$

$$\tan\delta_x = \frac{x_0\sqrt{1-g^2}}{\alpha_0 L + x_0(1-g)} \tag{20.17}$$

$$\tan\delta_y = \frac{y_0\sqrt{1-g^2}}{\beta_0 L + y_0(1-g)} \tag{20.18}$$

In general, the points where the rays intersect the mirror lie on an ellipse whose shape is determined by the launching conditions and the resonator set-up. For $\delta_y - \delta_x = k\pi$ the rays trace a circle, and for $\delta_y - \delta_x = (k+1/2)\pi$ a linear alignment is obtained (Fig. 20.12).

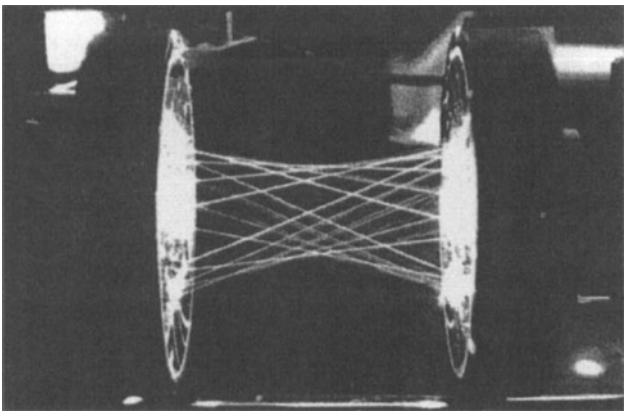

Fig. 20.13 The beam of an argon laser in a multipass Herriot cell used for stimulated Raman scattering (courtesy of Laser- und Medizin-Technologie Berlin gGmbH, Berlin, Germany).

In addition to their application in annular gain lasers, multipass Herriot cells have also been used as optical delay lines to increase the cavity round trip time. Effective resonator lengths of several kilometers have been achieved [S.25]. A further application of the Herriot cell is stimulated Raman scattering (SRS). The long interaction length with the gas significantly reduces the pump power required to achieve SRS threshold and high conversion efficiency [5.140] (Fig. 20.13).

20.4 Unstable Resonators

20.4.1 Toric Unstable Resonators

Similar to stable resonators with toric mirrors, the transverse modes of toric unstable resonators are closely related to those of unstable strip resonators with cylindrical mirrors [5.146]. The toric mirrors are obtained by rotating an arc of a circle about the optical axis (Fig. 20.14). The common parameters which describe conventional unstable resonators, namely the magnification M and the equivalent Fresnel number, also apply to toric unstable resonators. A further similarity to conventional unstable resonators is the applicability of geometric optics to predict the mode structure and the output coupling losses in the first order. By using geometrical beam propagation, a set of self-reproducing radial intensity distributions $I_p(r)$ at the output coupler can be found, given by [5.146]:

$$I_p(r) = const. \frac{(r-r_0)^{2p}}{r} \tag{20.19}$$

where r_0 is the radius of the mirror vertex and p is the radial mode order.

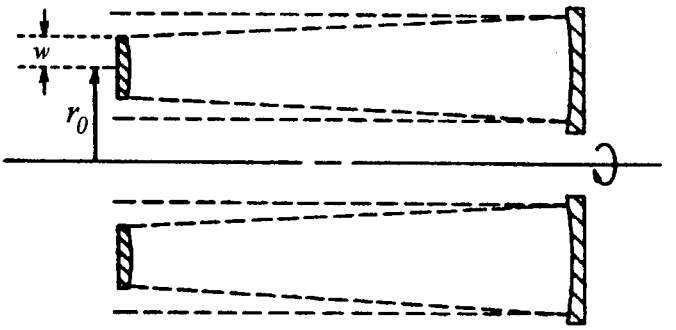

Fig. 20.14 Toric Unstable Resonator [5.146] (© OSA 1984).

These geometrical eigenmodes exhibit a round trip loss factor (=1-loss) of:

$$V_p = \frac{1}{M^{2p+1}} \tag{20.20}$$

where M is the magnification. For high equivalent Fresnel numbers, the actual intensity profile of the lowest loss mode will converge towards the $1/r$ distribution given in (20.19) for $p=0$, and the round trip loss is that of a strip resonator. Higher order modes will generally not be observed due to the high radial mode discrimination. For lower equivalent Fresnel numbers, the geometric approach is not suitable, and the mode structure has to be calculated using diffraction theory. If $u_p(x)$ denotes the transverse field distribution of the p-th eigenmode in the equivalent unstable strip resonator, the transverse field distributions of the eigenmodes of toric unstable resonators can be approximated by:

$$E_{p\ell}(r,\phi) = \frac{1}{\sqrt{r}} u_p(r-r_0) \exp[\pm i\ell\phi] \tag{20.21}$$

where r_0 is the radius of the mirror vertex. Since the output coupling loss is generated only in the radial direction, all azimuthal modes experience the same loss and no azimuthal mode discrimination is provided. The correct solution of the diffraction integral shows that there is a dependence of the radial mode profile on the azimuthal mode order, but this diffraction effect is too small to discriminate low order azimuthal modes. Therefore, the simultaneous oscillation of multiple azimuthal modes is to be expected unless mode selecting apertures are inserted into the resonator. As discussed in 20.2, the presence of azimuthally structured modes poses a serious problem as far as the focusability is concerned. On-axis intensity in the focal plane can only be generated with $\ell=0$ modes.

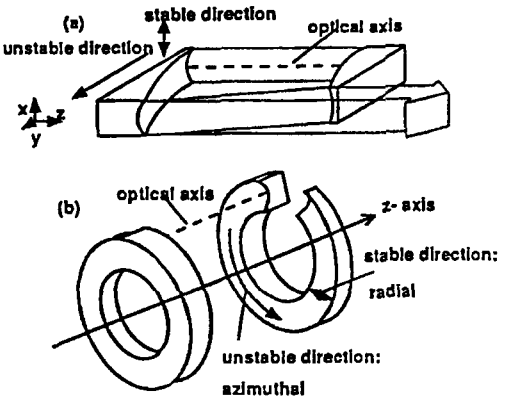

Fig. 20.15 Azimuthally unstable resonator (b). If the resonator is unwound, a one-dimensional off-axis unstable resonator is obtained (a) [5.167] (© SPIE 1994).

20.4.2 Azimuthally Unstable Resonators

The lack of azimuthal mode discrimination in toric unstable resonators is basically a result of the resonator being unstable in the radial direction. Improved mode properties should thus be expected if the azimuthal direction is chosen as the unstable direction [5.167,5.170]. Such an azimuthally unstable resonator can be obtained by winding an off-axis unstable resonator around the optical axis, as shown in Fig. 20.15. In the radial direction either a flat-flat or a stable resonator can be chosen since the radial dimension of the annulus is usually small enough to limit the radial mode order to low values.

Instead of using a parabolic mirror surface in the azimuthal direction, near diffraction limited beam quality can also be achieved with a helical output coupling mirror [5.167,5.170]. The set-up of a helical resonator is similar to that shown in Fig. 20.15b, except that the output coupling mirror has a constant slope in the azimuthal direction. In a geometrical model, the rays in the resonator are driven towards the output coupling aperture by the helical surface. However, the resonator is not unstable in the usual sense. Since the helical mirror is the annular version of a tilted flat mirror, the output coupling losses are given by the diffraction losses of a misaligned stable resonator and no geometric optics approximations for the mode structure exist like for unstable resonators. The output coupling can be increased with the slope of the helical mirror. For CO_2 lasers, typical slopes are on the order of $10\mu m/2\pi$. Measured and calculated intensity profiles in the near and the far field of a helical mirror CO_2 laser resonator are presented in Fig. 20.16. This resonator provided a maximum output power of 1,100W (the maximum total efficiency of 9% was attained at 450W) and beam parameter products close to the diffraction limit [5.170]. Note that for both resonator concepts, the output beam is highly astigmatic and beam shaping is necessary to generate round focus spots.

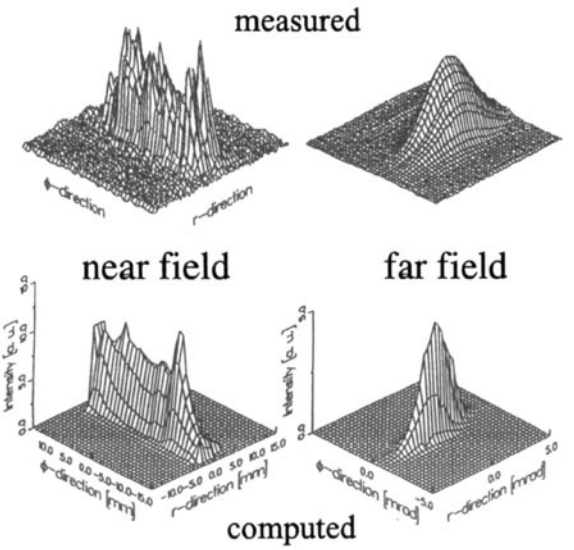

Fig. 20.16 Measured and calculated intensity distributions in the near field and the far field of an annular resonator with a helical output coupling mirror. Resonator length: 1.36m, discharge length: 1.15m, inner radius $a=48mm$, outer radius $b=55mm$ [5.170] (© IEEE 1994).

The application of azimuthally unstable resonators is currently limited by the fabrication of the resonator mirrors. For mid- to far-infrared lasers, the mirrors can be made of metal and flexible diamond turning techniques are available that are capable of generating non-rotationally symmetric surfaces. However, it is difficult to achieve optical surface quality and a commercial availability of these mirrors is not yet in sight. In the visible and the near-infrared spectral region, where glass is the preferred substrate material and a tighter tolerance on the surface roughness must be met, no successful manufacturing of toric or helical mirrors with optical quality has been reported yet.

An alternate annular resonator scheme that uses mirrors which are already available and that provides near diffraction limited beam quality is the tilted annular resonator as depicted in Fig. 20.17 [5.166]. Instead of a helically shaped mirror, a tilted toric or flat output coupling mirror is used. By using two flat mirrors, this resonator concept is also applicable to solid state lasers [5.161]. Similar to the helical resonator, the intracavity rays are guided towards the output coupling aperture. Unfortunately, no discrimination between the positive and the negative azimuthal direction is provided. Consequently, two nonparallel beams emerge from the aperture (Fig. 20.18). In order to achieve unidirectional operation, one of the beams can be reflected back into the resonator with an external mirror. Two times diffraction limited beam quality at a maximum output power of 700W (7% total efficiency) was reported for a diffusion-cooled CO_2 laser utilizing a tilted annular resonator [5.166]. A similar resonator provided a maximum output power of 2kW [5.165]. Output coupling in this resonator scheme is also present without tilting the resonator mirrors [5.169]. For the

aligned resonator, the azimuthal radiation flux is solely induced by the diffraction at the output coupling aperture. Unidirectional operation can be achieved through the mirror alignment (Fig. 20.19), but random jumping between one and two output beams is observed for slight mirror tilts. In [5.169], the unidirectional energy flux could be stabilized in an annular CO_2 laser by inserting diffuse-reflecting copper strips at different locations on the circumference of the mirrors. An output power of 250W at a total efficiency of 7.8% and beam propagation factors M^2 between 2 and 4 were reported.

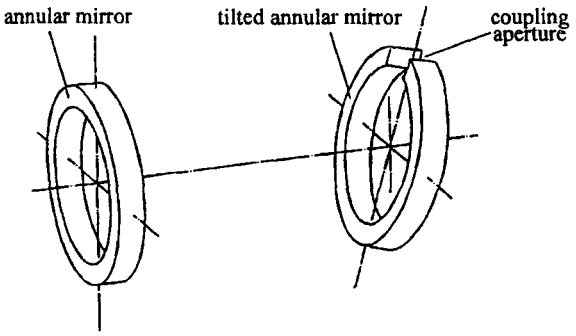

Fig. 20.17 Annular resonator with toric mirrors and an off-axis output coupling aperture. The tilt of the output coupling mirror induces a bidirectional azimuthal energy flux towards the aperture [5.166] (© IEEE 1993).

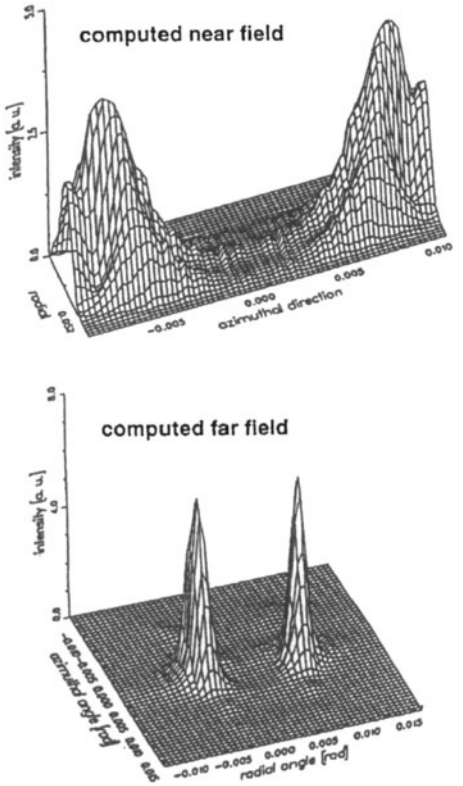

Fig. 20.18 Calculated near and far field intensities of a tilted annular resonator. The wave vectors of the two beams are not parallel, resulting in two peaks in the far field [5.166] (© IEEE 1993).

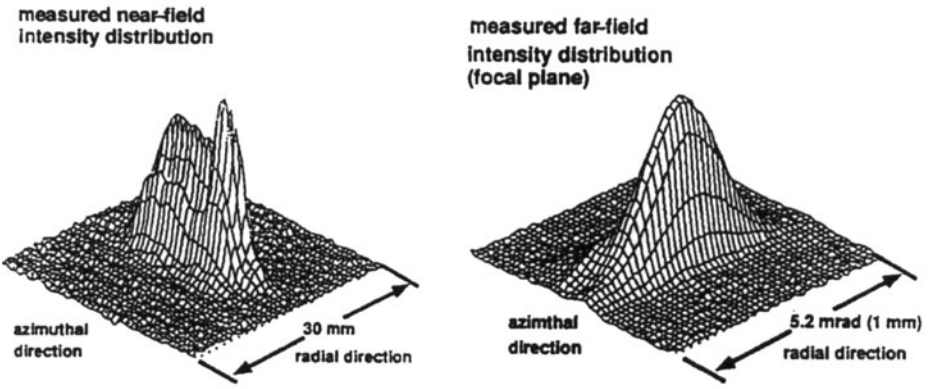

Fig. 20.19 Measured near field and far field intensity distributions for an annular resonator like the one depicted in Fig. 20.17, but with both mirrors aligned. An annular CO_2 discharge with an outer diameter of 110mm, a gap width of 7mm, and a length of 1.15m was used. The output coupling mirror was flat with an angular width of the aperture of 24°. The far field was recorded in the focal plane of a 7.5" focusing lens. Output power: 250W, pump power: 3.2kW [5.169] (© OSA 1994).

20.4.3 Spherical Unstable Resonators

If the unstable resonator comprises spherical mirrors, the intracavity beam has to be adapted to the annular shape of the active medium by using axicons, waxicons, or scrapers. The first experimental investigations of annular resonator geometries were focused on spherical unstable resonators because toric mirrors were not available at the time [5.131-5.137,5.139-5.144]. Some of these resonator schemes are presented in Fig. 20.20. The converging wave resonator uses a standard confocal unstable resonator placed outside the active region to form the mode. In the dual leg set-up shown in Fig. 20.20a, the feedback through the active medium is provided by a high reflecting mirror and a flat feedback mirror. The feedback arm excites the converging wave of the unstable resonator. After a couple of round trips the converging wave reaches the diffraction limited spot size and transforms into a diverging wave. After the diverging wave is subsequently expanded, a fraction of the power is coupled out and a fraction is reflected into the feedback arm. Diffraction limited beam quality has been attained with the converging wave resonator [5.134]. However, this resonator scheme suffers from parasitic oscillation between the flat mirror and the concave spherical mirror as well as from a high misalignment sensitivity. The linear version of the converging wave resonator shown in Fig. 20.20c exhibits similar problems.

A high alignment sensitivity is also a drawback of the HSURIA scheme depicted in Fig. 20.20b [5.141]. Furthermore, the complicated polarization properties of axicons and waxicons lead to a deterioration of the beam quality [5.142,5.164].

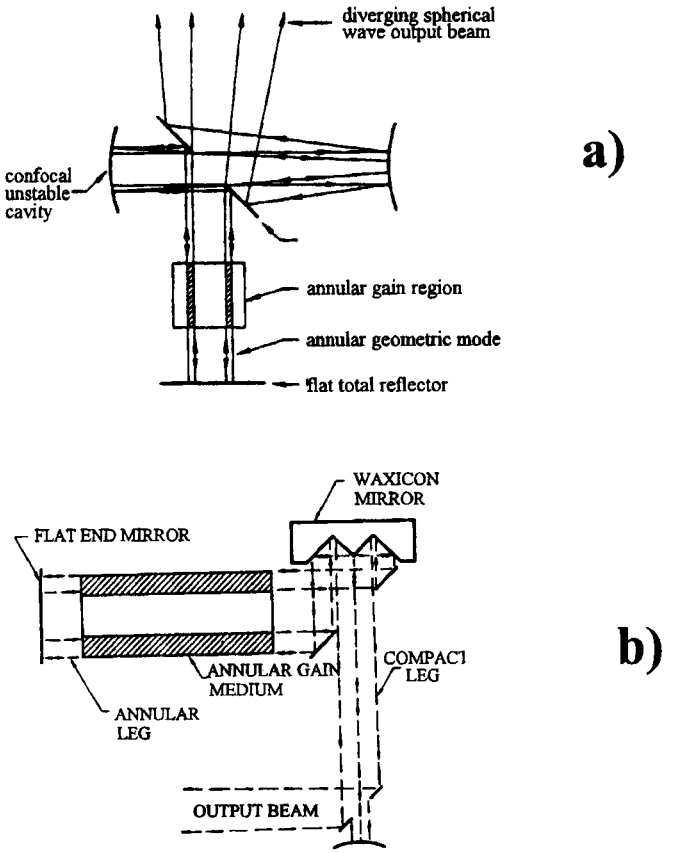

Fig. 20.20 Spherical unstable resonators for annular gain media. a) converging wave unstable resonator [5.134] (© OSA 1976), b) half-symmetric unstable resonator with intracavity axicon (HSURIA) [5.141] (© OSA 1980), c) linear converging wave unstable resonator.